Wang, M. and Chen, Q. 2009. "Assessment of various turbulence models for transitional flows in enclosed environment," Accepted by *HVAC&R Research*.

Assessment of Various Turbulence Models for Transitional Flows in Enclosed Environment (RP-1271)

Miao Wang
ASHRAE Student Member

Qingyan Chen; Ph.D.[1]
ASHRAE Fellow

Optimal control of enclosed environment requires detailed information of air distribution that could be obtained by numerically solving Navier-Stokes equations with a suitable turbulence model. This investigation evaluated the performance of eight turbulence models for transient airflow in enclosed environment using experimental data obtained in a room. The study used the room to create three cases with gradually added flow features, which were jet, separations, and thermal plumes. The flow regimes were transitional. The study found that some RANS models were good for simple flows, but not for complicated ones. The LES model was the most accurate and stable. The DES model under predicted turbulence kinetic energy near the walls. If the DES model included the subgrid-scale turbulence kinetic energy, the results can be significantly improved. This study shows the advanced features of LES and DES models for solving airflow in enclosed environment.

INTRODUCTION

HVAC systems for enclosed environment, such as commercial and residential buildings, medical facilities, industrial plants, vehicle and aircraft cabins, and entertainment facilities, are to provide suitable environmental conditions for its occupants or industrial processes. In order to create a suitable environment, air distribution parameters of the enclosed environments, including air velocity, air temperature, turbulence, and airborne species concentration etc, should be properly controlled. One of the tasks of HVAC system designers is to control the air distributions.

However, the control of the air distributions in the enclosed spaces can be very complex. One approach to achieve an optimal control is to model the distributions. In many enclosed spaces, the geometry of an air supply inlet, thermal boundary conditions, and furniture could cause complicated flow features. Such flow features are difficult to be modeled correctly. For example, in the region near an air supply inlet, the flow is typically turbulent. In the downstream, the turbulence could delay and relaminization

[1] Miao Wang is a Research Assistant and Qingyan Chen is a Professor, Herrick Laboratories, School of Mechanical Engineering, Purdue University, West Lafayette, IN 47907.

may occur. Thus, the airflow in a room with a weak jet could contain the combination of turbulent, laminar and transitional flow. Thermal buoyancy from occupants could form unstable plumes. Large quantity of furniture could cause flow separations. Many existing modeling techniques have failed to calculate accurately the transitional flow, unstable plumes, and separated flows (Zhang et al. 2007).

Thus, this study intends to find a suitable model that can be used to investigate the flow features and to model air distributions in enclosed spaces for optimal designs. Due to rapid growth in computer capacity and speed, Computational Fluid Dynamics (CFD) has become the most widely used technique for airflow modeling in enclosed spaces (Zhai et al. 2007, Chen 2008). By solving conservation equations of mass, momentum, energy, and species concentrations, CFD can predict steady or transient air distributions with rich details, which are helpful to design HVAC systems.

The accuracy of CFD modeling depends on many factors, such as discretization scheme, numerical methods, boundary conditions, and turbulence models. For example, Zhang et al (2007) systematically evaluated eight turbulence models for indoor airflow simulations. The models include an indoor zero equation model (0-eq) (Chen and Xu, 1998), a low Reynolds number k-ε model (LRN) (Launder and Shamar, 1974), an RNG k-ε model (RNG) (Yakhot and Orszag, 1986), an SST k-ω model (SST) (Menter, 1994), a v^2f model (v2f) (Davidson et al, 2003), a Reynolds stress model (RSM) (Gibson and Launder, 1978), a detached-eddy-simulation model (DES) (Shur et al, 1999), and a large-eddy-simulation model (LES) (Germano et al, 1996; Lilly, 1992). When these models were applied to simulate natural, forced and mixed convections, the result show that the LES and DES models provide rich flow details, while the accuracy may not always be the best. The v2f and the RNG model are slightly better in some cases, but not always. They found that not a single model is superior to the others probably because these models were not specifically developed for enclosed spaces.

The study from Zhang et al. (2007) provides us the performance of the eight turbulence models in indoor airflow modeling. The flows studied were the combined results of many factors. For example, their forced convection included both jet flow and separation. When discrepancies were found between the calculated results and measured data, it was difficult to find out which factor made the turbulence model fail. For this reason the benchmark cases should be able to separate the flow characteristics. And the factors contributing to complex flow features should be studied one by one.

Most of the turbulence models tested by Zhang et al. were Reynolds Averaged Navier-Stokes (RANS) models. Their study had only one LES model and one DES model. The RANS models are usually developed and tuned for a specific type of flow. Their empirical coefficients in the models may not be appropriate if flow conditions change. The LES and DES theories have more solid fluid physics than the RANS models, and contain only one or no empirical coefficient. The LES and DES models should be more universal. The LES and DES models deserve further investigation.

Therefore, the objective of this study was to investigate the factors causing complex flow features one by one and then to identify promising and advanced turbulence models for such flows. The first part of this study was to obtain high quality experiment data of complex flow in an enclosed space. The experiment should contain the complex flow

features, but the complexities should be added step by step. The second part was to test and develop a suitable turbulence model by using the experiment data as a benchmark.

EXPERIMENTAL STUDY

The purpose of this experimental study was to investigate complex flow features in rooms. The experiment should be representative to airflows in enclosed environments, and should include major flow characteristics, such as jets, separations, and thermal plumes. It was not desirable to use real enclosed spaces, since those cases may have too many uncertainties. Instead, simplified spaces, but still with complex flow features, were more favorable. The complexity of the flow features should be added step by step, which was useful to test the capacity of turbulence models.

EXPERIMENTAL TECHNIQUE

A test room of 8 ft × 8 ft × 8 ft (2.44 m × 2.44 m × 2.44 m) was used for this investigation as shown in Figure 1(a) based on a half of a twin-aisle airline cabin with three rows of seats and 10.5 passengers inside (Figure 1(b)). The model room had a jet, a box to represent furniture, and a heat source inside the box that could generate complex flows. A linear (slot) diffuser, which was located on the left wall near the ceiling, had an opening height of 1.25 in (0.03 m) along the whole width of the room. An exhaust slot with a height of 3 in (0.08 m) along the whole width was located near the floor on the right wall. The model room was built using insulation materials. The supply flow was provided by a pressure plenum of 8 ft × 8 ft × 2 ft (2.44 m × 2.44 m × 0.61 m) that could maintain a stable pressure. The pressure plenum used two layers of perforated metal inside to provide a uniform air velocity along the width of the slot opening. The supply airflow rate was controlled to be 210 cfm (0.10 m^3/s), which corresponded to 20 cfm (0.01 m^3/s) per passenger for an airline cabin. The supply air temperature was controlled at 72°F (22.2°C).

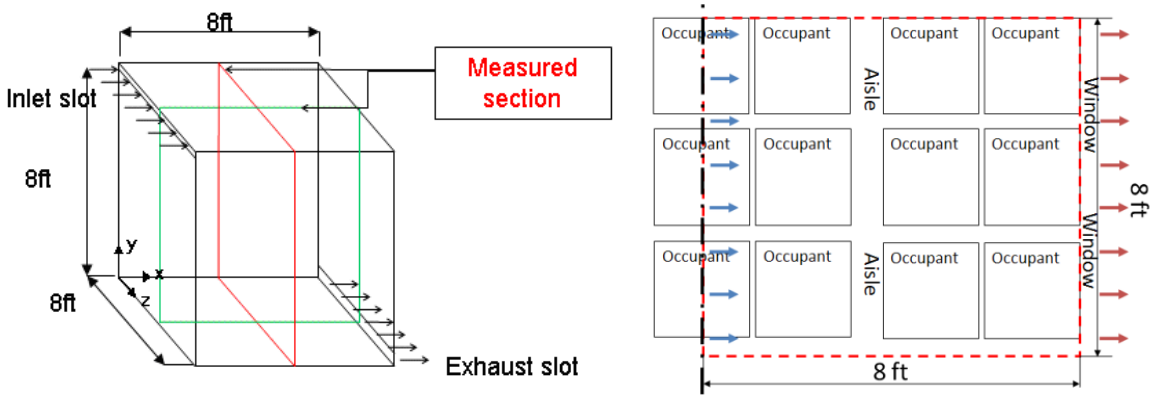

(a) (b)

Figure 1 The experimental facility used to study complex flow features in a room. (a) The model room. (b) Analogue to a half of a three rows, twin-aisle cabin.

This experiment lump-summed all the seats and passengers to a 4 ft × 4 ft × 4 ft (1.22 m × 1.22 m × 1.22 m) box. Inside the box, sixteen light bulbs were used to generate a heat source of 700 W that was equivalent to the sensible heat generated by the 10.5 passengers. When the box was heated, four fans inside the box were running to make the box surface temperature uniform. Under this heat load, the surface temperature was found to be 98°F (36.7°C).

In order to study different flow features, three test cases were designed to gradually increase the complexity of the flow features. The first case was an isothermal forced convection in the room without the box. The second case was with the box with the heat source and the third case was with the heated box as illustrated in Figure 2.

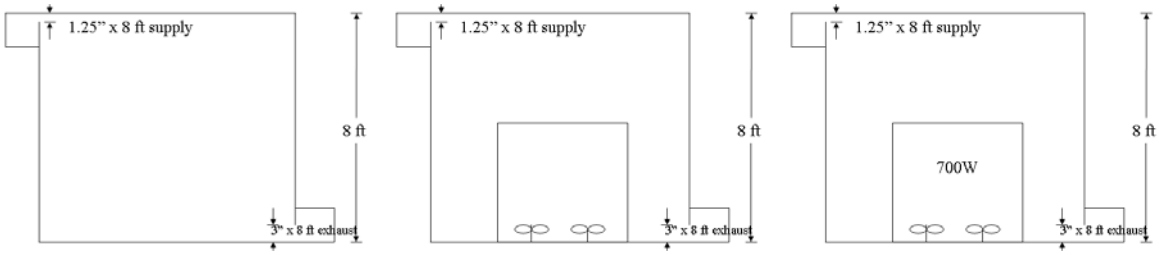

(a) Case (1) (b) Case (2) (c) Case (3)

Figure 2 Three experimental cases with gradually increase on flow complexity: (a) isothermal forced convection, (b) with a box representing furniture, and (c) with 700 W of heat sources inside the box.

Case (1): Isothermal forced convection in the empty room (Figure 2(a)).

This case was controlled to be isothermal. The forced convection was generated by the jet from the upper-left wall. The Reynolds number of the supply air based on the slot height was around 2600, which indicates that the flow was transitional. This case was designed to study the impact of inlet jet on the flow inside the room.

Case (2): Isothermal forced convection in the room with the box (Figure 2(b)).

Based on Case (1), this case included the box in the center of the room but without the heat source. All other settings were exactly the same as those in Case (1). Thus, Case (2) was also isothermal, which was designed to study the impact of the separations caused by the box.

Case (3): Mixed convection in the model room with the heated box (Figure 2(c)).

This case added 700 W of heat inside of the box. All other experimental conditions were exactly the same as those for Case (2). The heated box could form a thermal plume. This case was designed to study the influence of thermal buoyancy on the flows in the room.

In order to measure the spatial distributions of the air velocity and velocity fluctuation in the room, two ultrasonic anemometers were used to measure them at a stream-wise section and a cross section as shown in Figure 1(a). The ultrasonic anemometers measured instantaneous velocity in three perpendicular directions with a frequency of 20 Hz. The anemometer measured the air velocity of an air parcel about 2 in × 2 in × 2 in (0.05 m × 0.05 m × 0.05 m), which was surrounded by the six sensors of the anemometer. The accuracy of the anemometers was 0.005 m/s with ±1% error for velocity, which is caused by volume averaging.

The flow was measured with a 6-in (0.15 m) grid resolution. This grid resolution could capture all the flow structures in the room. It is not meaningful to have a resolution finer than six inches because the sensor was pretty bulky (two inches in diameter). Thus, there were a total of 512 measuring points for the two sections in Case (1) and 384 measuring points for Case (2) or Case (3). The total points were fewer for Cases (2) and (3) because of the box in the room. The two ultrasonic anemometers can measure at two points once. Each measurement took five minutes to obtain 6000 data entries (20 Hz × 300 s), with which the mean and fluctuation velocities can be obtained. After the sensors were moved to other positions, the flow in the room was stabilized for at least 12 minutes before taking another set of data.

Although the ultrasonic anemometers could measure air temperature when measuring the air velocity, the temperature data were not useful. This was because the measurements for one case took several weeks, and the variation of outdoor temperature over this period could have a significant impact on the indoor air temperature. In order to solve this problem, 16 thermal couples were used for the temperature measurements. The temperature measurements took about two hours for one case, during this period the temperature in the room was stable.

The experiment also measured the boundary conditions. Since the height of inlet slot was only 1.25 in (0.03 m), the ultrasonic anemometers were too bulky for measuring the inlet air velocity. The experiment used 16 omni-directional hot-sphere anemometers to measure the inlet air velocity, turbulence, and temperature at three different heights at a total of 48 positions. The anemometers were appropriate since the stream-wise air velocity component was absolutely dominant.

In order to obtain the thermal boundary conditions for CFD simulations, the surface temperature of the box, walls, floor, and ceiling were measured by an infra-red thermometer at 16 (= 4 × 4) positions on each surface.

This experiment used a tracer gas with 1% of SF_6 to measure the flow rate. The SF_6 gas was released at the mixing zone inside the room with a known flow rate, Q_{source}. The averaged SF_6 concentration at the exhaust, $C_{exhaust}$, and at the supply, C_{inlet}, were measured to determine the airflow rate Q from the slot inlet:

$$Q = \frac{C_{source}}{C_{exhaust} - C_{inlet}} Q_{source}$$

The average concentration of SF_6 in the room C, is ($C_{inlet} \approx 0$):

$$C = \frac{1\% \bullet Q_{source}}{Q}(1 - e^{-Qt/V})$$

where t is the time since the tracer gas is released, and V = 512 ft^3 (14.5 m^3) is the volume of the room, and Q is proximately 200 cfm (0.10 m^3/s). When t = 15 minutes, the SF_6 concentration reaches 99.7% of the equilibrium concentration. Therefore, the measurement began 20 minutes after the tracer gas was released, and took another 30 minutes for measurement.

The measured inlet velocity profiles were also used to calculate the flow rate.

EXPERIMENTAL RESULTS

All the measured and simulated results presented in this paper were non-dimensionlized. The length was normalized by the room size (L = 8 ft (2.44 m)), velocity by the maximum velocity found in the three cases (U_{max} = 295 fpm (1.5 m/s)), and turbulence kinetic energy (TKE) by the maximum TKE (k_{max} = 1937 ft^2/min^2 (0.05 m^2/s^2)). The dimensionless air temperature was defined as $T^* = (T-T_{min})/(T_{max}-T_{min})$, where T_{min} = 72°F (22.2°C) and T_{max} = 98°F (36.7°C) were the minimum and maximum temperature found in Case (3), respectively.

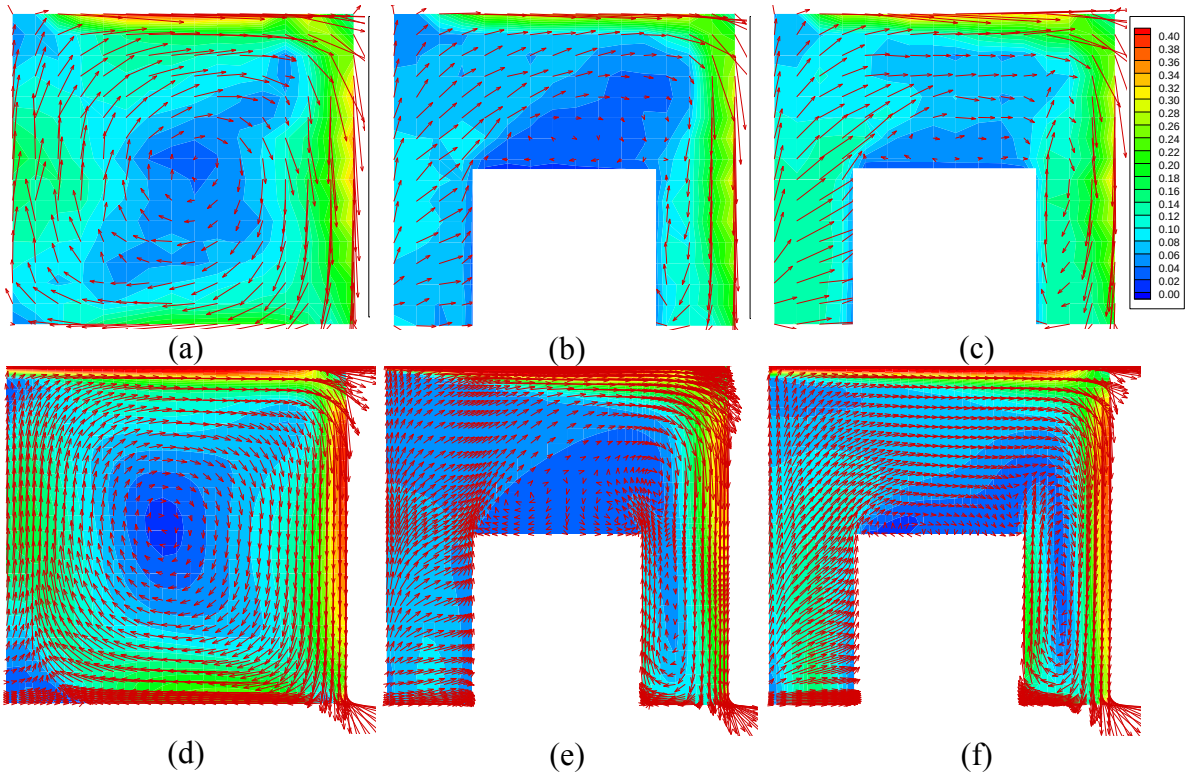

Figure 3 Measured and simulated velocity at the stream wise section. (a), (b), and (c): measured velocity of Case (1), (2), and (3) respectively. (d), (e), and (f): simulated velocity of Case (1), (2), and (3) respectively. U / U_{max}, where U_{max} = 295 fpm (1.5 m/s).

Error! Reference source not found.(a), (b), and (c) depict the measured velocity distributions at the stream-wise section of three cases. **Error! Reference source not found.**(d), (e), and (f) show the corresponding simulated velocity distributions that will be discussed later. The airflow entered the room from the inlet slot at the upper-left corner, and extracted through an exhaust slot at the lower-right corner. **Error! Reference source not found.**(a) shows a large clock-wise circulation. High velocity was found along the room enclosure, and the airflow in the center of the room was small. Although not shown here, the flow in the room was two dimensional. **Error! Reference source not found.**(b) illustrates that the flow contained two clockwise recirculations, one above the box and the other between the box and the right wall. **Error! Reference source not found.**(b) also shows that, between the left wall and the box, the airflow pointed to the right direction, which indicates a strong three-dimensional flow from the two sides. The heated box could enhance the upward flow due to the thermal buoyancy.

Comparing **Error! Reference source not found.**(a) with 3(b), the averaged velocity magnitude decreased by 35% due to the presence of the box, because the box acted as an obstacle in the flow field. If the box was heated, the velocity increased by 35%, as depicted in **Error! Reference source not found.**(c) since the buoyancy generated an important aiding momentum to the flow.

This investigation found that the turbulence intensities in all the cases were higher than 50%. This high turbulence level was mainly caused by the transitional flow. Figure 4(a), (b), and (c) show the turbulent kinetic energy in the stream-wise section for the three cases. Figure 4 illustrates that the turbulent energy in all the three cases was high in the jet region where the flow was clearly turbulent. In the recirculation zone at the center of the room, the turbulent energy was low that corresponded to laminar flow. Thus, the flows studied here were indeed transitional. The results also show that the turbulence was mainly created by the jet. The walls had a very strong damping effect, though they may also increase the turbulence by the steep velocity gradient.

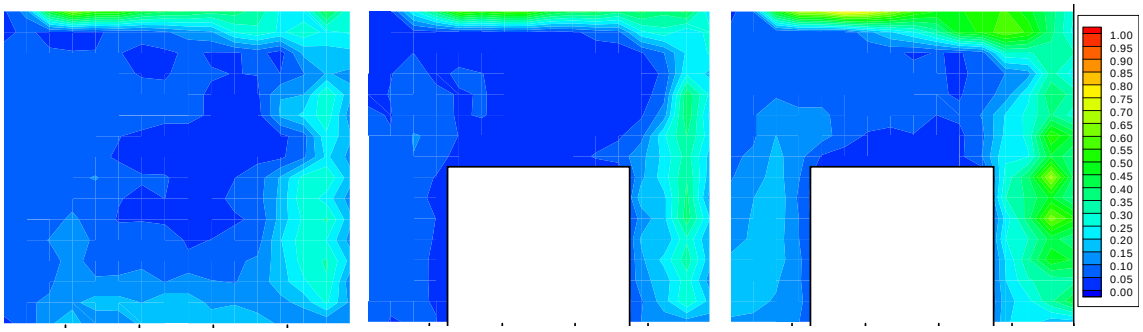

Figure 4 Measured turbulence at stream wise section of three cases. (a), (b), and (c): turbulence kinetic energy of Case (1), (2), and (3) respectively. k / k_{max}, where k_{max} = 1937 ft^2/min^2 (0.05 m^2/s^2).

With the box in the room, the turbulent kinetic energy decreased further as depicted in Figure 4(b). The wall surfaces of the box did create further damping effect near the surfaces. The box reduced the TKE by 20% in the room. However, the box created a

secondary recirculation in the cavity between the right box wall and the right room wall that led to a higher turbulence level in the cavity. When the box was further heated as shown in Figure 4(c), the buoyancy made the secondary recirculation even stronger so that the turbulence was the highest in the cavity. The thermal plume from the heated box increased the TKE in the room by 75%, which can be observed by comparing Figure 4(b) with Figure 4(c).

This study also measured the air temperature distribution in the mixed convection case, as shown in Figure 5. In the stream-wise section (Figure 5(a)), the cold air jet from the upper-left corner was heated when it flowed along the ceiling and the right wall. The heated box generated a strong thermal plume above it. Figure 5(b) shows that in the cross section the temperature profile was nearly symmetrical. The temperature distributions measured indicate that the air was not well mixed in the room, due to the strong thermal buoyancy and not so strong jet flow.

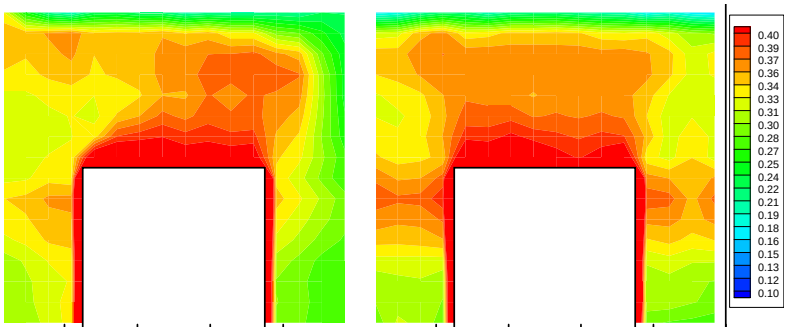

(a) (b)

Figure 5 Temperature distributions of the mixed convection case (Case (3)) in (a) Stream-wise section and (b) Cross section. $(T-T_{min})/(T_{max}-T_{min})$, where T_{min} = 72°F (22.2°C) and T_{max} = 98°F (36.7°C).

To summarize the airflow characteristics, this investigation found that the supply air jet generated a high turbulence level in the room but the wall surfaces had strong damping effect on turbulence. The box acted as an obstacle that decreased the velocity in the room. The box created a secondary recirculation, which enhanced turbulence level in the center of the recirculation zone. The buoyancy from the heated box also enhanced the recirculation and the turbulence in the room. The room air was not well mixed by the jet and thermal plume.

NUMERICAL STUDY

The aim of our study was to identify suitable turbulence models for calculating flows in buildings. The experimental study reported above provided detailed flow characteristics in a room with gradually added flow complexities. The experimental data can be used as a benchmark for identifying the models.

The numerical study simulated these experimental cases with various turbulence models. Since the complex flow features were added one by one in these experimental cases, it is possible to find out the model performance for each flow feature, which could also provide valuable information for model improvements.

There are three kinds of turbulence modeling techniques available: RANS modeling, LES, and DES that is a hybrid model of RANS and LES. The RANS modeling solves the time-average Navier-Stokes equation for the mean flow parameters and models turbulence parameters by a turbulence model. The LES solves filtered Navier-Stokes equations for large-scale flow parameters and models the subgrid-scale parameters. The DES uses LES for the main flow field and RANS model near the boundaries.

Zhai et al (2007) studied the three turbulence modeling techniques. The models they tested were either widely used or proposed mainly for indoor airflow modeling. Zhang et al (2007) tested one zero-equation, three two-equation, and one three-equation eddy-viscosity model; one Reynolds stress model; one LES model; and one DES model for various indoor airflows. The eight models they tested are shown in Table 1 with "*".

Their study concluded that the RNG k-ε model and the v2f model had best performance for the natural, forced, and mixed convection cases. The LES model provided more flow details but not the most accurate. However, their test cases may not be representative for indoor airflow. For example, they used natural convection case in a tall cavity, which is not usually found in enclosed spaces. In addition, their test cases included many flow features at a same time, which made it difficult to find out the influence of flow features on the model performance. Further, Zhang et al. tested only one LES and one DES, which may not be sufficient to fully explore the model potentials.

Therefore, our numerical study tested turbulence models using cases obtained from our experimental study. In addition to the eight turbulence models, our study added two LES subgrid scale models and two DES models as listed in Table 1. One of the LES subgrid scale model was the wall-adapting local eddy-viscosity model, which returns the wall asymptotic behavior of wall bounded flows. The other was the dynamic kinetic energy subgrid-scale model, which calculates the subgrid scale turbulence viscosity by solving a transport equation of subgrid scale turbulence kinetic energy. One of the DES models was a combination of the Realizable k-ε model and the LES, the other was a combination of the SST k-ω model and LES. The four additional models were among the most widely used LES and DES models. It would be essential to find out the performance of these models for indoor airflow modeling.

Table 1 Turbulence models used in this study

Turbulence models		**Tested Models**
EVM	Zero eqn	Indoor zero eqn. (0-eq) (Chen and Xu, 1998) *
	Two eqns	RNG k-ε (RNG) (Yakhot and Orszag, 1986) * Launder-Sharma (LRN) (Launder and Sharma, 1974) * SST k-ω (SST) (Menter, 1994) *
	Three eqns	v2f-Davidson (v2f) (Davidson et al, 2003) *
RSM		IP (RSM) (Gibson and Launder, 1978) *

LES	Dynamic Smagorinsky SGS Model (LES-DSL) (Germano et al, 1996; Lilly, 1992) * Wall-Adapting Local Eddy-Viscosity SGS Model (LES-WALE) (Nicoud and Ducros, 1999) Dynamic Kinetic Energy SGS Model (LES-ke)(Kim andMenon, 1997)
DES	DES Spalat-Allmaras (DES-SA)* (Shur et al, 1999) DES SST k-ω (DES-SST) (Strelets, 2001; Menter et al, 2003) DES Realizable k-ε (DES-ke) (FLUENT, 2006; Shih et al, 1995)

* Models tested by Zhang et al. (2007)

NUMERICAL TECHNIQUE

This study used a commercial CFD code FLUENT (version 6.3) for identifying suitable turbulence models for indoor airflows. All of the turbulence models were already available in FLUENT except the modified v2f model, which was implemented by adding three transport equations for turbulence parameters via user-defined functions.

For the RANS models, the SIMPLE algorithm was adopted to couple pressure and momentum equations. The PRESTO! scheme was used for pressure discretization, and the second-order upwind scheme was used for all other variables. The solutions were converged when the sum of normalized residuals for all the cells became less than 10^{-6} for energy and 10^{-3} for all other variables. (FLUENT, 2006) The normalized residuals are defined as:

$$R^{\phi} = \frac{\sum_{cells\,P} \left| \sum_{nb} a_{nb}\phi_{nb} + b - a_P\phi_P \right|}{\sum_{cells\,P} \left| a_P\phi_P \right|}$$

where, ϕ_P and ϕ_{nb} are the flow variable of the present and neighboring cells respectively, a_P is the center coefficient, a_{nb} are the influence coefficients for the neighboring cells, and b is the contribution of the constant part of the source term and of the boundary condition. This investigation solved only steady-state equations for RANS modeling.

For the LES and DES, the algorithm, discretization schemes, and convergence criteria were the same as those for the RANS modeling except the discretization technique for the momentum equation. The discretization used the bounded central differencing scheme. The LES and DES were first used to calculate the transient flows for five minutes to reach a statistically stable state, and then for another five minutes to obtain statistically steady-state solutions. The time step for LES and DES were adjusted to ensure that the number of iterations for each time step was between five and ten (Fluent, 2006).

Our study first examined the grid independence and investigated the grid meshes of all the models for the three cases. The LES and DES models required fine grids with y+ in the order of 1 for the first cells near a wall. The finer a grid was, the more accurate the result would be. The grid numbers for the RANS models were usually coarser than that for the LES or DES. Sufficiently fine grids were also needed to eliminate the numerical

error. Different models should have different grid distributions near a wall. This investigation used two approaches for a wall: one approach modeled directly the flow near a wall that required fine mesh distribution, and the other used the logarithmic wall function that needs the y+ value at the first grids to be between 30 and 50. Table 2 lists the grid resolutions, y+ values, and wall treatments for all the models. Note that this study used non-uniform grid distribution with finer grids near a solid wall, and coarser far from the wall. As an example, Figure 6 depicts the grid convergence study with the v2f model for Case (1). In this particular location the case with 72×72×72 grids seems slightly better than that with 44×44×44 grids. In fact, at other locations, the case with 44×44×44 grids could be better than that with 72×72×72 grids. Therefore, the results with 44×44×44 grids were regarded as similar to those with 72×72×72 so that the 44×44×44 grids were considered to be sufficiently fine for further studies.

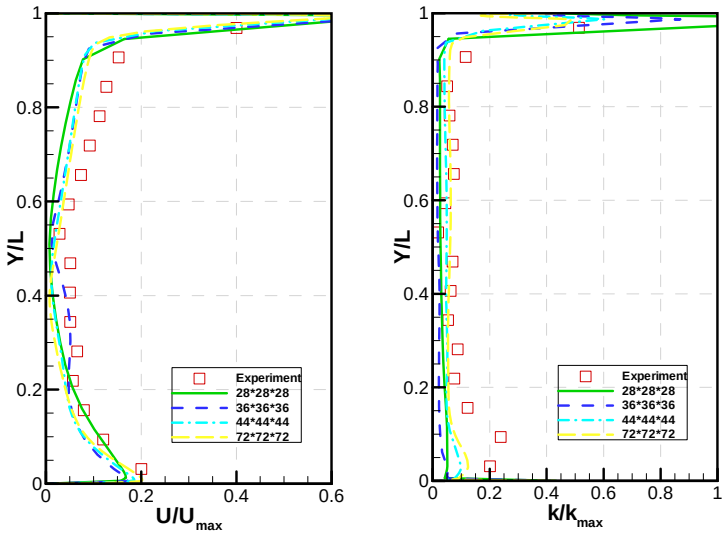

Figure 6 Grid dependence study for Case (1) with the v2f model. (a) Velocity profile at x=45 in and z=48 in and (b) the profile of turbulence kinetic energy at x=45 in and z=48 in.

NUMERICAL RESULTS

This study compared the simulated and measured velocity distributions to assess the performance of turbulence models. For example, **Error! Reference source not found.**(d), (e), and (f) show the simulated velocity distributions of Cases (1), (2), and (3) with the v2f model. In general, the velocity distributions were very similar to the measured ones. It is difficult to make quantitative comparison in **Error! Reference source not found.**. This study also compared the calculated results with the measured data at ten representative positions in the room, as shown in Figure 7. The ten positions represent two sections that should contain most important information of the flow. Due to limited space available, this paper shows detailed comparison for Case (1) at three of the ten positions corresponding to the best, worst, and average model performance. Note that the

three positions may vary from case to case. The paper reports the results at only one representative location for the other two cases.

Table 2 Mesh information and wall treatments used for the eight turbulence models

Model	Case	Grid resolution	Typical y^+	Wall treatment
0-eq	1	44×44×44	8	Resolved
	2	44×44×44	8	
	3	72×72×72	5	
LRN	1	44×44×44	8	Resolved
	2	44×44×44	8	
	3	44×44×44	8	
RNG	1	36×36×36	30	Wall Function
	2	36×36×36	30	
	3	44×44×44	25	
SST	1	28×28×28	35	Wall Function
	2	36×36×36	30	
	3	36×36×36	30	
v2f	1	44×44×44	20	Resolved
	2	44×44×44	20	
	3	44×44×44	20	
RSM	1	44×44×44	30	Wall Function
	2	36×36×36	30	
	3	44×44×44	30	
LES-DSL	1	77×96×77	1	Resolved
	2	110×77×101	1	
	3	110×77×101	1	
DES-SA	1	77×96×77	1	Resolved using RANS model
	2	110×77×101	1	
	3	110×77×101	1	

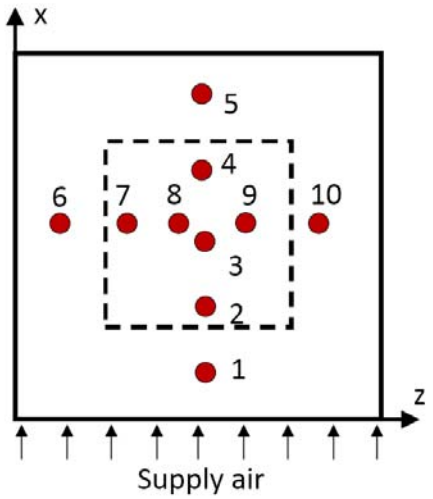

Position	Coordinate (x inch, y inch)	Position	Coordinate (x inch, y inch)
1	(0.2286, 1.2192)	6	(1.2192, 0.2286)
2	(0.6858,1.2192)	7	(1.2192, 0.6858)
3	(1.1430,1.2192)	8	(1.2192, 1.1430)
4	(1.6002,1.2192)	9	(1.2192, 1.6002)
5	(2.0574,1.2192)	10	(1.2192, 2.0574)

Figure 7 Ten positions in the room where the comparison of the computed and measured results were made

Case (1): Forced convection in the empty room.

In this case, the geometry and flow were relatively simple. The top and bottom figures in Figure 8 were for the same position but with different models in order to make the figures more readable. As shown in Figure 8(c), the 0-eq model provided an acceptable velocity prediction in general. The major discrepancies between the simulated and measured data was found in position 5, where the inlet flow reached to the opposite wall, and went down to the floor. At this position, the flow was with strong curvature and had separations. The simple 0-equation model could not handle such a complex flow in the region. The predicted velocity profiles by the RNG, LRN, RSM, and SST models were similar, which also agreed well with the experimental data. Since this was a relatively simple airflow, the flows used to obtain the empirical coefficients for the models could be similar to that in this case. Thus, it was not very surprising to see the good performance of these eddy viscosity models. The v2f model under-predicted the air velocity profiles in many positions. The LES-DSL and DES-SA models produced similar but also acceptable results. Unfortunately, the LES-DSL model did not perform as well as many of the RANS models.

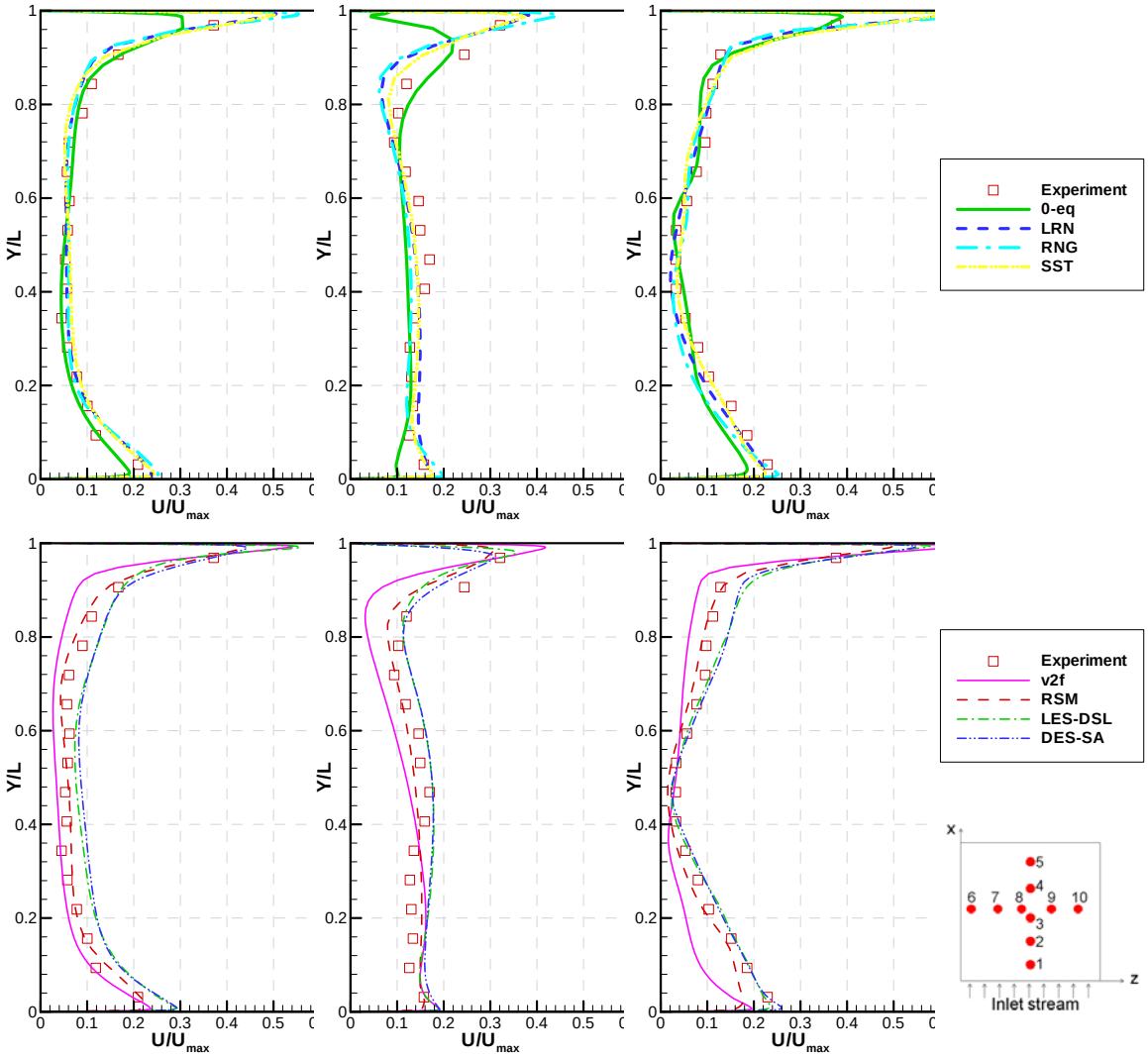

(a) Best (position 4) (b) Worst (position 5) (c) Average (position 6)

Figure 8 Velocity profiles predicted by the eight turbulence models for Case (1): (a) best position, (b) worst position, and (c) average position.

For turbulence kinetic energy (TKE) shown in Figure 9, the indoor 0-eq model did not solve the TKE thus it cannot be included in the comparison. The SST model tended to over-predict the TKE. The LRN, RNG, and RSM models can predict well the TKE. For the LES-DSL and DES-SA models, the TKE was computed from the resolved velocity fields. The TKE profiles obtained with the v2f, LES-DSL, and DES-SA model were acceptable, although some discrepancies existed between the computed and measured TKE near the wall. The DES-SA model also under-predicted the TKE near the ceiling where the model switched to RANS mode and the model did not perform well.

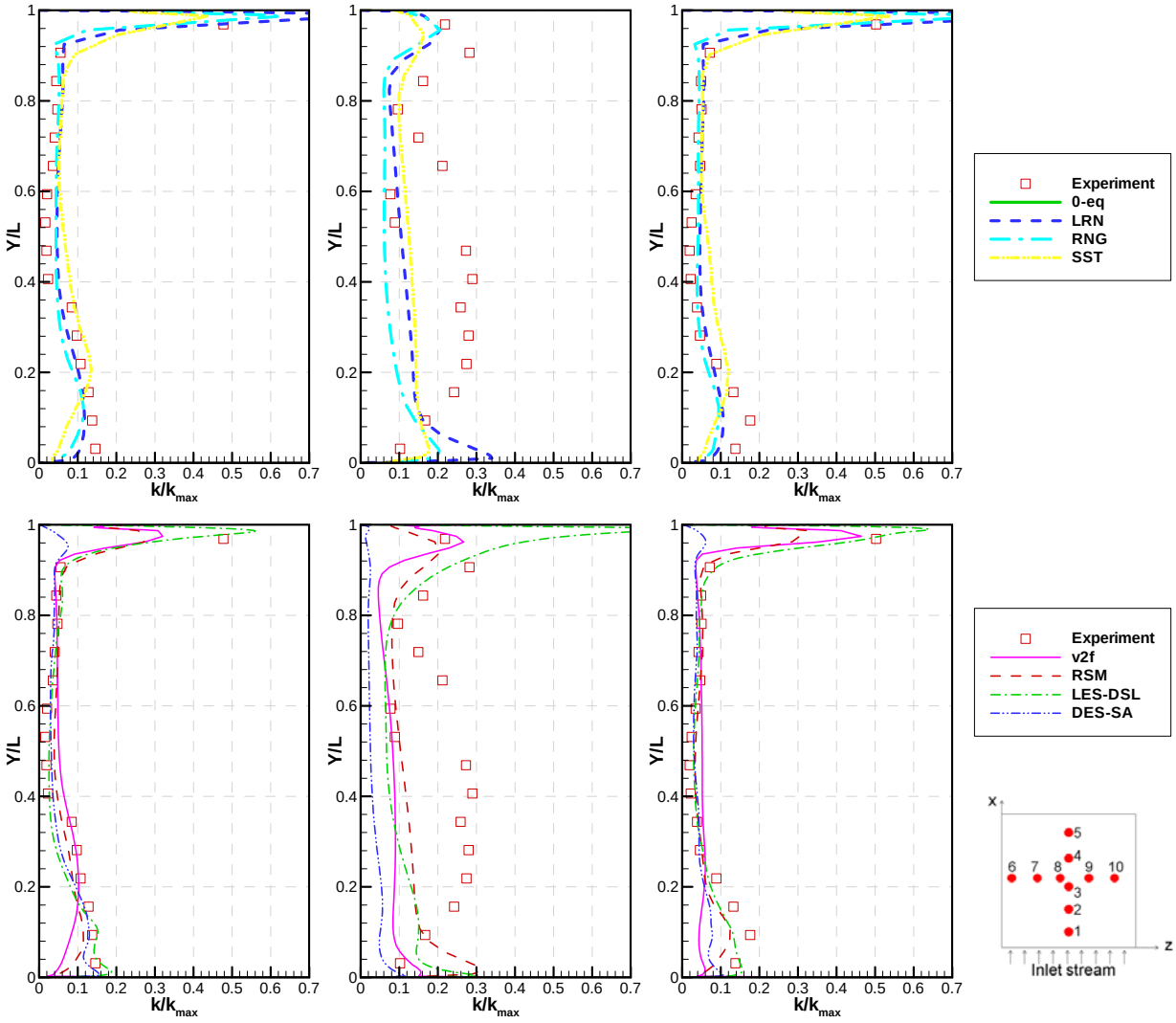

(a) Best (position 10) (b) Worst (position 5) (c) Average (position 6)

Figure 9 Turbulence kinetic energy profiles predicted by the eight turbulence models for Case (1): (a) best position, (b) worst position, and (c) average position.

Case (2): Forced convection with the box in the room

In this case, the box placed in the room caused flow separations. Figure 10 shows the results for position 6 that is typical among the 10 positions. The 0-eq model provided a fairly good prediction on the air velocity compared with other more advanced RANS models. It was remarkable for such a simple model. Although it was not shown here, most of the eddy viscosity models under predicted the air velocity especially at position 5. At position 5, the flow was very complicated since the box and the jet interacted and generated a secondary recirculation. The performance of the SST model was particularly poor. The v2f model did a very good job for this case. Its anisotropic formulation of eddy viscosity made it suitable for flow bounded with many walls. The RSM model worked pretty well, since it solved Reynolds stresses in different directions. Its anisotropic nature led to good performance for flows with strong curvature. The LES-DSL model in this

case can predict well the air velocity, but the performance of the DES-SA model remained the same as Case (1).

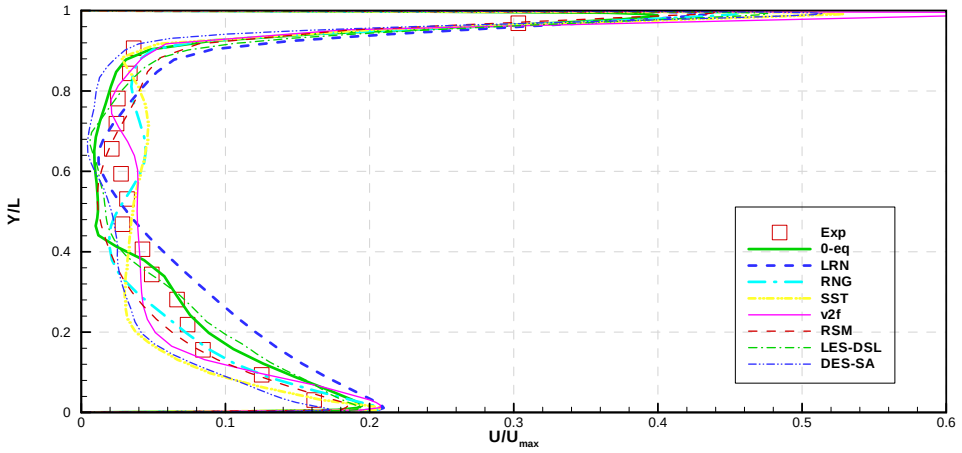

Figure 10 Velocity profiles predicted by the eight turbulence models for Case (2) at position 6.

As shown in Figure 11, the RNG, SST, v2f, and RSM models gave reasonable predictions of the TKE. The LRN model over predicted the TKE at many locations. Most of the RANS models did a poorer job for Case (2) than for Case (1) because the flow features became more complicated. The LES-DSL model provided the best predictions for the TKE, while the performance of the DES-SA model was stable. From the stability point of view, the LES models are superior to the RANS models.

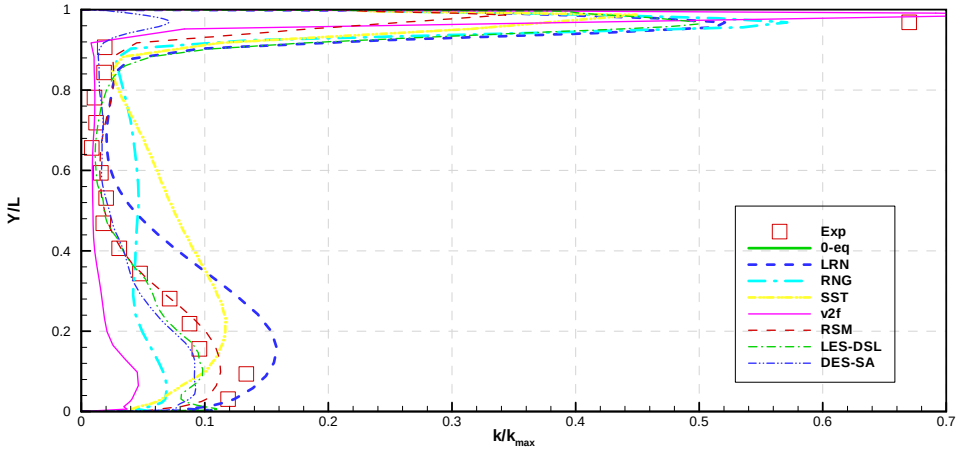

Figure 11 Turbulence kinetic energy profiles predicted by the eight turbulence models for Case (2) at position 6.

Case (3): Mixed convection with a heated box in the room

Figure 12 shows the performance of the eight models in predicting the air velocity. Again, position 6 represents the typical results for this case. The 0-eq model did not

produce a smooth profile in many positions and the results did not agree with the experiment data well. The simple algebraic formation to determine turbulence viscosity used in the model failed in the mixed convection case. The LRN model also over predicted the velocity at many locations. The SST model failed to predict velocity correctly at some locations. The RNG and RSM model showed acceptable accuracy in predicting the velocity. The v2f model performed the best among the RANS models. The LES-DSL was the best among all the models.

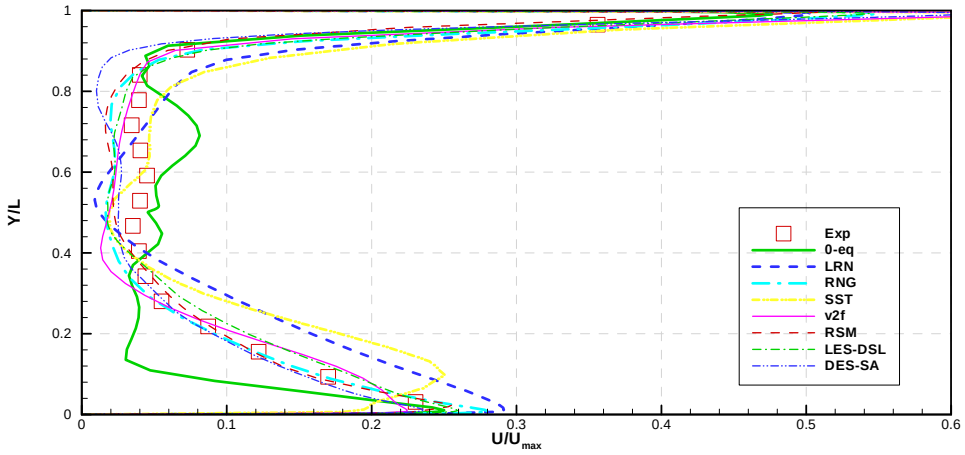

Figure 12 Velocity profiles predicted by the eight turbulence models for Case (3) at position 6.

The typical results for the TKE are shown in Figure 13. The LRN model over predicted the TKE at many locations; its performance dropped significantly when the heat was introduced. The RNG, SST, v2f, and RSM models gave acceptable TKE profiles, but under predicted turbulence near the ceiling. These RANS models failed where the shear stresses were large. The LES-DSL predicted most accurate result at most of the locations for turbulence. The DES-SA model, once again, under predicted the TKE near the ceiling. However, if an advanced DES model were used to take the subgrid TKE into account, the result could be improved significantly, which would be discussed in the next section.

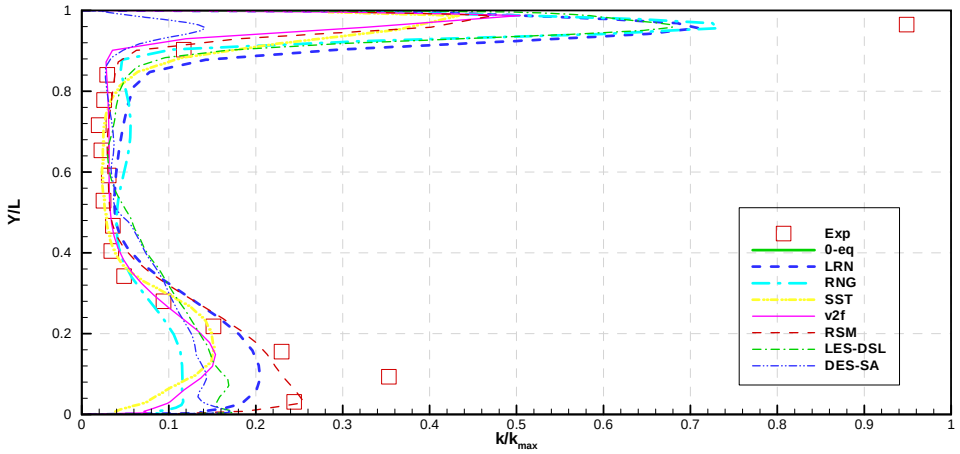

Figure 13 Turbulence kinetic energy profiles predicted by the eight turbulence models for Case (3) at position 6.

The air temperature profiles as shown in Figure 14 were mainly influenced by the velocity prediction. The RNG, v2f, RSM, and LES-DSL models predicted good results. Though the SST model failed to correctly predict velocity magnitude, the trend of its velocity prediction was correct that may have contributed to a good temperature prediction. The DES-SA model was not as good as the above models, but was still acceptable. The results of the 0-eq, and LRN models were fair, simply because these two models predicted wrong trends of velocity.

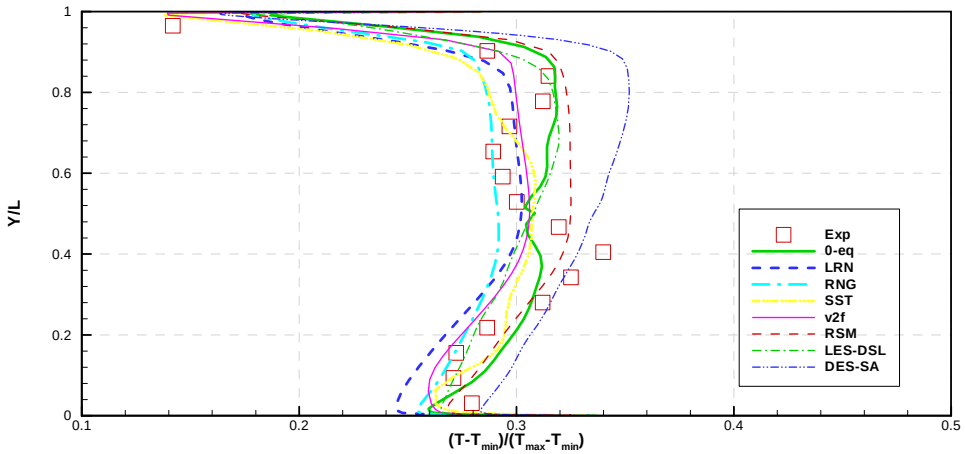

Figure 14 Temperature profiles predicted by the eight turbulence models for Case (3) at position 6.

Please note that this study used the RNG k-ε model with 101x87x110 grids for this flow. The simulations were used as initial fields for the LES model. When comparing the results for the fine grids with those for the coarser grids, the fine grids gave the worst velocity prediction at some locations for unknown reason. However, the simulations by the RNG k-ε model with 36x36x36, 44x44x44, and 72x72x72 grids gave pretty consistent and similar results. This was another reason the results with 44x44x44 grids were presented in this paper.

DISCUSSION

Table 3 summarizes the performance of the eight models. The models were rated as A, B, C, or D according to the relative errors between the simulated results and the experiment data. The grade is A with an error smaller than 10%, B with an error between 10-30%, C with an error between 30-50%, and D with an error greater than 50%. If the trend of the results went to the wrong direction, the rating was down one more grade further.

Table 3 gives the overall grades for the eight models in predicting all the flow parameters for the three cases. Many of the RANS models did not receive a high grade. Even for the two best RANS models, RNG and RSM models, their performance dropped as the flow complexity increased. If they were applied to even more complex airflow in real indoor environment, their performance may be worse.

Table 3 Performance of the eight turbulence models for the three flow cases

Cases	Item	Turbulence models							
		0-eq	LRN	RNG	SST	V2f	RSM	LES-DSL	DES-SA
1	U	B	A	A	A	C	A	B	B
	TKE	N/A	A	A	C	B	A	B	B
2	U	A	B	B	C	A	A	A	B
	TKE	N/A	C	B	B	B	B	A	B
3	U	D	D	B	C	A	B	A	A
	TKE	N/A	C	B	B	B	B	A	B
	T	C	C	A	A	A	A	A	B
Overall grade		2.5	2.6	3.4	2.9	3.3	3.6	3.7	3.1

U: mean air velocity, TKE: turbulence kinetic energy, T: mean air temperature.

A: Good (4.0), B: Acceptable (3.0), C: Marginal (2.0), and D: Unacceptable (1.0).

The overall grade of the LES-DSL model was the highest due to its good performance in Cases (2) and (3). Its stable performance was impressive and showed a great potential for indoor airflow modeling. However, the LES-DSL model calculated the subgrid-scale eddy viscosity using a simple algebraic equation.

$$\mu_t = \rho L_s^2 \left|\overline{S}\right|$$

where L_s is the mixing length and $\left|\overline{S}\right| = \sqrt{2\overline{S}_{ij}\overline{S}_{ij}}$.

Subgrid-scale eddy viscosity plays a very important role in airflow simulation. Such a simple model may not be sufficient for complex flows. In order to test this assumption, this study further tested two LES models with advanced subgrid-scale models: the LES-WALE and LES-ke model as shown in Table 1. The LES-WALE model calculates subgrid-scale eddy viscosity that can return the wall asymptotic behavior of wall bounded flows. The LES-ke model determines subgrid-scale viscosity by solving a transport equation of kinetic energy. The test used the mixed convection case (Case (3)), since it is the most complicated one among the three cases.

Figure 15 compares the results of the two advanced LES models with those of the LES-DSL model at position 6. Again, the position was representative. Figure 15(a) shows that the velocity profiles predicted by the LES-DSL and LES-ke models were comparable and more accurate than the LES-WALE model. However, the discrepancies among the three models were small. Figure 15(b) shows the air temperature profiles. None of the models perfectly predicted the air temperature profile, but the errors of three models were not

evident. Figure 15(c) depicts the TKE profiles predicted by the three models. The discrepancies were not significant except the ceiling and floor regions where the grid distributions were not sufficiently fine to resolve small-scale turbulence.

In general, all the three LES models worked well in Case (3). The relative simple LES-DSL model did a pretty good job. Different LES models had small discrepancies on the resolved TKE. The discrepancies on the air velocity and temperature were larger, but still insignificant. It was because if the grid distribution were sufficiently fine to resolve small flow motion, the subgrid-scale model would become unimportant.

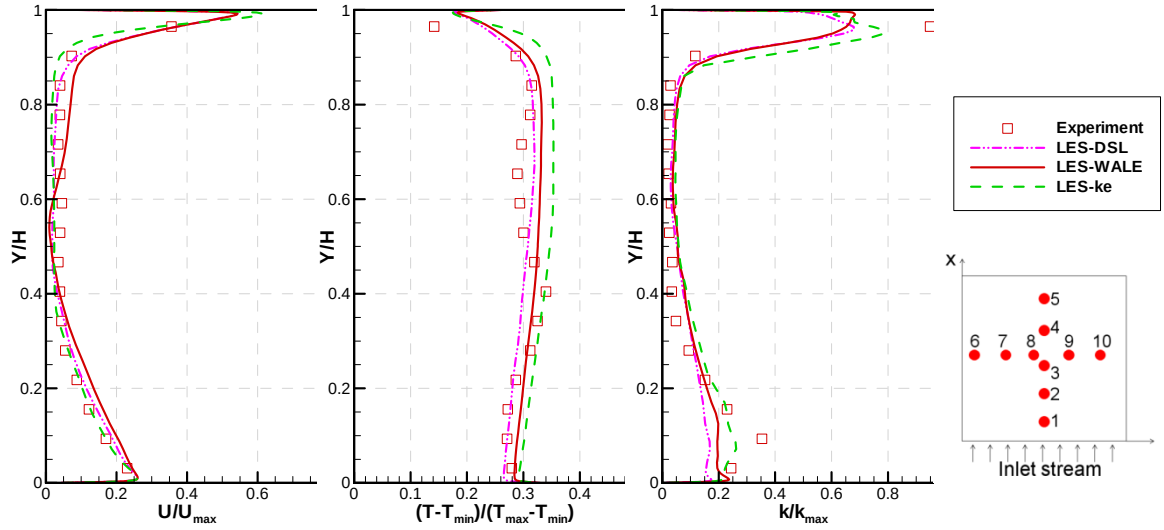

Figure 15 Comparison between three LES subgrid-scale models for Case (3) in predicting (a) velocity magnitude, (b) turbulence kinetic energy, and (c) temperature.

On the other hand, Table 3 also shows that the DES-SA model was very stable although the grade was in the middle. The poor TKE prediction was probably caused by the RANS model it used in boundary layers that did not solve TKE but turbulent viscosity. Namely, the DES-SA model uses Spalart-Allmaras model for boundary layers, which calculates turbulence viscosity by:

$$\mu_t = \rho \bar{\upsilon} f_{v1}$$

where ρ is the density, f_{v1} is a damping function, and $\bar{\upsilon}$ is solved by a transport equation. The turbulence viscosity could not be used to determine the TKE. Thus, the TKE profiles shown for the three cases do not include the modeled TKE.

Some other DES models use different RANS models, such as the DES-ke and DES-SST models, that determine subgrid-scale TKE. This study tested these two models for Case (3) to assess the impact of the modeled TKE on the total TKE. The DES-ke model solves two additional transport equations, one for subgrid-scale TKE, and the other for turbulence dissipation rate ε. Similarly, the DES-SST model solves for subgrid-scale TKE, and specific dissipation rate ω.

Figure 16 shows that both the models successfully predicted the TKE profile by adding the subgrid-scale TKE into it. Their resolved TKE and modeled TKE profiles were also shown separately in the figure. Near the ceiling region, the major part of the TKE was from the modeled subgrid-scale TKE. The two DES models worked in slightly different ways in switching between RANS and LES mode. In the middle part of the room, the modeled TKE with the DES-SST model was more important than the resolved one, while that with the DES-ke model was the opposite. This difference was probably due to the different switching techniques used.

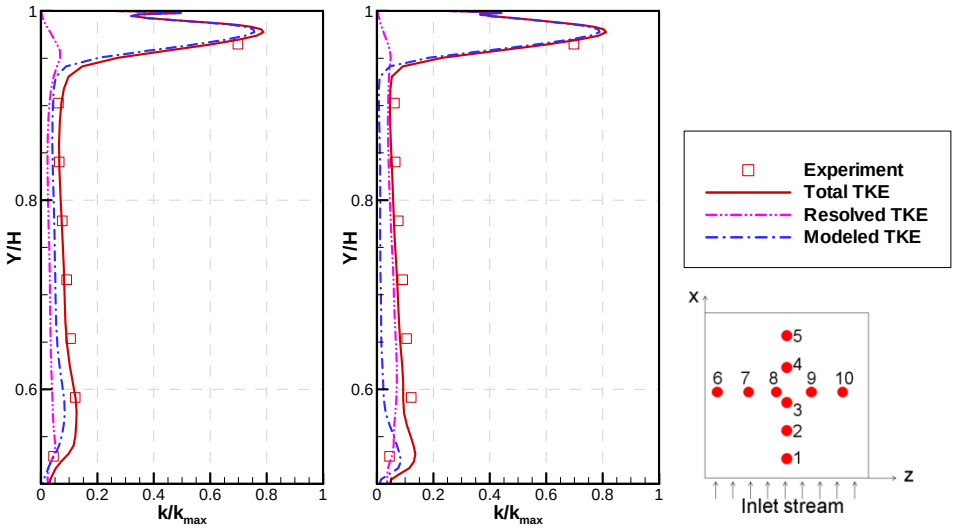

(a) (b)

Figure 16 Different turbulence kinetic energy profiles in position 2 for Case (3) (a) DES-SST model and (b) DES-ke model.

CONCLUSIONS

This investigation studied experimentally basic airflow features found in indoor environments. Three test cases were designed to study the complexity of the airflow features step by step in a room. The study found that the inlet jet generated a high turbulence level in the room. The wall had a strong damping effect on the turbulence in the room air. A box that simulated furniture in the room acted as an obstacle and can decrease the velocity and turbulence levels in the room air due to its wall damping effect. The buoyancy generated from the heated box enhanced the air recirculation thus the velocity and turbulence levels.

The experiment data was then used to evaluate the performances of eight different turbulence models. Among the six RANS models, the RNG and RSM models had a good overall performance, but their accuracy suffered as the flow became more complex. The other RANS models had mixed performance. The LES-DSL model was the best among the eight models. The performance of the DES-SA model was stable.

Two more LES models were further tested to study the impact of subgrid scale models on predicting the three flows. The results show that the subgrid-scale models had very similar performance. Our study has also tested two different RANS models used in DES for predicting the TKE. The subgrid-scale TKE was important if one wants to obtain correct TKE profiles for the flow.

ACKNOWLEDGEMENT

The authors would like to express their gratitude to Technical Committee 4.10 "Indoor Environment Modeling" of American Society of Heating, Refrigerating and Air-Conditioning Engineers, Inc. for initiating this research and to its Project Monitoring Subcommittee for their help and numerous suggestions to the study presented in this paper.

NOMENCLATURE

0-eq	= zero equation model	LES-WALE	= Wall-Adapting Local Eddy-Viscosity SGS Model
DES	= detached eddy simulation	LRN	= low Reynolds number k-ε model
DES-ke	= DES Realizable k-ε model	RANS	= Reynolds average Navior-Stokes
DES-SA	= DES Spalat-Allmaras model	RSM	= Reynolds stress model
DES-SST	= DES SST k-ω model	RNG	= RNG k-ε model
EVM	= eddy-viscosity model	SGS	= subgrid-scale
LES	= large eddy simulation	SST	= SST k-ω model
LES- DSL	= Dynamic Smagrinsky SGS model	TKE	= turbulence kinetic energy
LES-ke	= Dynamic Kinetic Energy SGS Model	V2f	= v^2f Davidson model

SUBSCRIPTS

exhaust	= value at the exhaust	source	= value at the source
inlet	= value at the inlet	nb	= neighboring cells
P	= present cell		

SYMBOLS

C	= concentration (ppm)	source	= value at the source
k	= turbulence kinetic energy	T	= temperature
Q	= volume flow rate (m^3/s)	U	= velocity

REFERENCES

Chen, Q., and Xu, W. 1998. A zero-equation turbulence model for indoor airflow simulation. *Energy and Buildings* 28(2):137-144.

Chen, Q. 2009. Ventilation performance prediction for buildings: A method overview and recent applications. *Building and Environment* doi:10.1016/j.buildenv.2008.05.025.

Davidson, L., Nielsen, P.V. and Sveningsson, A. 2003. Modification of the v2f model for computing the flow in a 3D wall jet. *Turbulence, Heat and Mass Transfer* 4:577-84.

FLUENT. 2006, FLUENT 6.3 Documentation, Fluent Inc., Lebanon, NH.

Germano, M., Piomelli, U., Moin, P., and Cabot, W. H. 1996. Dynamic Subgrid-Scale Eddy Viscosity Model. In Summer Workshop, Center for Turbulence Research, Stanford, CA,.

Gibson, M.M., and Launder, B.E. 1978. Ground effects on pressure fluctuations in the atmospheric boundary layer. *Journal of Fluid Mechanics* 86:491-511.

Kim, W.-W., and Menon, S. 1997. Application of the localized dynamic subgrid-scale model to turbulent wall-bounded flows. Technical Report AIAA-97-0210, American Institute of Aeronautics and Astronautics, 35th Aerospace Sciences Meeting, Reno, NV, January.

Launder, B.E., and Sharma, B.I. 1974. Application of the energy dissipation model of turbulence to the calculation of flow near a spinning disk. *Letters in Heat Mass Transf*er 1:131-38.

Lilly, D. K. 1992. A Proposed Modification of the Germano Subgrid-Scale Closure Model. *Physics of Fluids* 4:633-635.

Menter, F. R. 1994. Two-equation eddy-viscosity turbulence models for engineering applications. *AIAA journal* 32:1598-605.

Menter, F. R., Kuntz, M., and Langtry2003. R. Ten Years of Experience with the SST Turbulence Model. In K. Hanjalic, Y. Nagano, and M. Tummers, editors, *Turbulence, Heat and Mass Transfer* 4:625-632. Begell House Inc.

Nicoud, F., and Ducros, F. 1999. Subgrid-Scale Stress Modelling Based on the Square of the Velocity Gradient Tensor. *Flow, Turbulence, and Combustion* 62(3):183-200

Shih, T.-H., Liou, W. W., Shabbir, A., Yang, Z., and Zhu, J. 1995. A New - Eddy-Viscosity Model for High Reynolds Number Turbulent Flows - Model Development and Validation. *Computers Fluids* 24(3):227-238.

Shur, M., Spalart, P. R., Strelets, M., and Travin, A. May 1999. Detached-Eddy Simulation of an Airfoil at High Angle of Attack. In 4th Int. Symposium on Eng. Turb. Modeling and Experiments, Corsica, France.

Spalart, P.R. 2000. Strategies for turbulence modelling and simulations. *The International journal of heat and fluid flow* 21.3 (2000) , 252-263.

Strelets, M. 2001. Detached Eddy Simulation of Massively Separated Flows. AIAA, Aerospace Sciences Meeting and Exhibit, 39 th. Reno, NV.

Yakhot, V., and S.A. Orszag. 1986. Renormalization group analysis of turbulence. *Journal of Scientific Computing* 1:3-51

Zhai, Z.Q., Zhang, W., Zhang, Z., and Chen, Q. 2007. Evaluation of various turbulence models in predicting airflow and turbulence in enclosed environments by CFD: part 1 - Summary of prevalent turbulence models. *HVAC&R RESEARCH* 13 (6):853-870.

Zhang, Z., Zhai, Z.Q., Zhang, W., and Chen, Q. 2007 Evaluation of various turbulence models in predicting airflow and turbulence in enclosed environments by CFD: Part 2-comparison with experimental data from literature. *HVAC&R RESEARCH* 13(6): 871-886.